15. N. A. Zheltukhin, V. I. Zapryagaev, A. V. Solotchin, and N. M. Terekhova, "Spectral composition and structure of stationary vortical Taylor–Görtler disturbances of a supersonic underexpanded jet," Dokl. Russian Academy of Sciences, 325, No. 6 (1992).
16. N. A. Zheltukhin and N. M. Terekhova, "Taylor–Görtler instabilities in a supersonic jet," PMTF, No. 5 (1993).
17. J. M. Floryan, "On the Görtler instability of boundary layers," Prog. Aerospace Sci., 28, 235 (1991).
18. V. Ya. Borovoi, V. V. Ivanov, A. A. Orlov, and V. N. Kharchenko, "Visualization of three-dimensional flow over models with the aid of a laser knife," Uchen. Zap. TsAGI, 4, No. 5 (1973).

TAYLOR–GÖRTLER INSTABILITY IN A SUPERSONIC JET

N. A. Zheltukhin and N. M. Terekhova

UDC 532.526+533

This paper is devoted to the numerical modeling of the characteristics and structure of a new (for supersonic jets) class of disturbances and some applications of the results to the interpretation of the experimental data presented in [1-3]. The object of this paper is to obtain basic data and to verify the model of the existence of the Taylor–Görtler instability in a free supersonic flow. The literature available to us does not contain any information about such investigations. This work is a detailed exposition of the results presented briefly in [3, 4].

We consider first the hypothesis that the flow contains stationary rotational disturbances of the type Taylor–Görtler waves (T–G), excited by additional centrifugal forces arising due to the curvature of the trajectories of the gas following the real cellular "barrel-shape" structure of a nonisobaric jet. This choice, from among existing alternative choices, one of which is described in [5], is dictated by the following circumstances. First, longitudinal bands, indicating the existence of azimuthal nonuniformities of the optical density, are recorded near the nozzle cutoff, where the trajectories of the gas are actually curvilinear. Second, under the experimental conditions (underexpanded jet with degree of underexpansion $N \sim 5$) a wide-band spectrum of noise is recorded; this precludes the appearance of strong nonlinear effects at such early stages, and the other nonlinearities will be second-order infinitesimals compared to the linear T–G waves. The weak effect of sharp gradients at the nozzle cutoff flow discontinuities is indicated by the fact that the intensity of the bands decreases with increaing surface smoothness under constant efflux conditions.

So, the hypothesis that stationary rotational disturbances exist in the initial section of the jet is most plausible. Within the framework of this hypothesis we performed numerical modeling of the characteristics of the waves, studied the dependences on the flow parameters, and analyzed the experimental data in order to retrieve the local values of the density and velocity of the flow.

1. Equations for the Disturbances. The flow scheme within the first cell ("barrel") of the jet is displayed in Fig. 1. A system of linearized equations for T–G-wave-type disturbances, which includes a number of assumptions to be discussed below, was constructed in [5]:

$$\begin{gathered} Uv_x' - [2Uu'/R_0] + p_r'/\rho_0 = 0, \quad Uw_x' + p_\varphi'/r\rho_0 = 0, \\ Uu_x' + U_r v' + [Uv'/R_0] + p_x'/\rho_0 = 0, \quad U(p'/a^2 - \rho')_x - \rho_{0r} v' = 0, \\ U\rho_x' + \rho_{0r} v' + \rho_0 (v_r' + w_\varphi'/r + u_x' + v'/r + [v'/R_0]) = 0. \end{gathered} \tag{1.1}$$

This system was constructed for a one-dimensional flow of a compressible, nonviscous, heat-nonconducting gas with the velocity field $\mathbf{u} = |\varepsilon v', \varepsilon w', U + \varepsilon u'|$, where v', w', u' are, respectively, the transverse, azimuthal, and longitudinal, components of the disturbances in the coordinates r, φ, and x; ρ' and p' are the disturbances of the density and pressure, respectively; $U = U(r)$ is the longitudinal component of the average velocity; ρ_0 is the

Novosibirsk. Translated from Prikladnaya Mekhanika i Tekhnicheskaya Fizika, No. 5, pp. 48-55, September-October, 1993. Original article submitted November 13, 1992.

 0021-8944/93/3405-0640$12.50

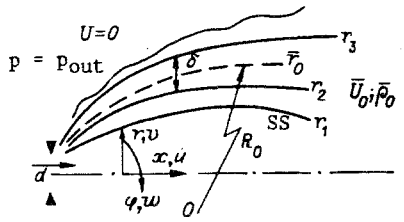

Fig. 1

average flow density; and, a is the local sound speed. The equations were represented in dimensionless form by scaling the variables to the following characteristic quantities: $\bar{r}_0$ is the radial coordinate where the velocity is half its maximum value (U = 0.5); $\bar{U}_0$, $\bar{\rho}_0$ are, respectively, the maximum velocity and the density in the initial mixing layer.

The additional forces, which are proportional to $1/R_0$ (R_0 is the radius of curvature of the trajectories of the gas), are enclosed in brackets. The value of R_0 determines the centrifugal effects and the associated T–G waves. The system (1.1) is valid as a local approximation under the condition R_0 = const. As one can see from Fig. 1, R_0 changes in magnitude due to the growth of the boundary layer and the corresponding arrangement of the streamlines within the first "barrel." Determining the value of R_0 is itself a problem, which did not arise for flows near walls. The first and natural variant is to determine R_0 from sharp visible or measured reference points, such as the position of the suspended shock (SS) or the line of maximum total pressure p_0 in the compressed layer. This is apparently not entirely correct. Gas from the surrounding flooded space plays in the jet the role of a solid wall, on which all disturbances stop, and although the oscillations are mainly concentrated in the mixing layer, they can penetrate quite far into this space, thereby perturbing it. The values of R_0 calculated along the lines of asymptotic decay of disturbances differ significantly from the values of R_0 obtained from the exact reference points, and since the concept of radius of curvature is basic for analytical descriptions of T–G waves, an attempt must be made to find reasonable agreement between these values.

2. Average Flow. We study the problem in the plane-parallel approximation. It is acknowledged that in order to describe T–G waves in subsonic flows near walls the transverse component of the average velocity V must be included in the calculations [6]; doing so ensures that diffusion and viscous effects are taken into account correctly. For a nonisobaric supersonic jet this component must be neglected at this stage due to the fact that there are no reliable data on the form and magnitude of V on the initial section of the jet [7]. The profile of the longitudinal component U is taken, just as in [5], from experimental approximations [8]. Doing so, of course, introduces into the results errors that cannot yet be estimated.

The compressed layer itself (r_1–r_3 in Fig. 1) consists of two subregions [9]. In the first subregion, from the suspended shock r_1, the total pressure is restored up to its maximum value on the line r_2. This value is used as the start of the mixing layer (its inner boundary). Next, p_0 and therefore the average velocity U decrease to their values in the flooded space ($p_0 \sim p_{out}$, $U \approx 0$). The coordinate r_3 is the conventional exterior boundary of the mixing layer, whose thickness $\delta = r_3 - r_2$. The half-velocity point virtually coincides with the half-width δ of the layer, so that $r_2 = 1 - \delta/2$ and $r_3 \gtrsim 1 + \delta/2$, and $U(r_3) \sim 0.06$. Thus

$$U(r) = \begin{cases} 1 & r < r_2, \\ \exp(-0.693\eta^2) & r \geqslant r_2, \end{cases}$$

where the self-similar coordinate $\eta = 2(r - r_2)/\delta$. The relation between the average density ρ_0 and U was determined from the gas-dynamic relation $\rho_0 = [1 + M_0^2(1 - U^2)(\varkappa - 1)/2]^{-1}$, where $\varkappa = c_p/c_V$ (M_0 is the Mach number with $U = \bar{U}_0$). A modification of Sutherland's formula [8] can also be employed; this is virtually equivalent. The sound speed $a = (\rho_0 M_0^2)^{-1/2}$.

In this work the structure of the acceleration section $r_1 \leqslant r \leqslant r_2$ was neglected, since it was assumed that in regions with positive velocities gradients $dU^2/dr > 0$, in accordance with the results of [6], the flow is more stable against T–G perturbations than in regions with $dU^2/dr = 0$.

3. Form and Eigenvalues of T–G Waves. The solutions of the system (1.1) can be obtained by two methods. In the first method, the linearized equations are directly integrated

numerically. This method is still more problematic than the second method, in which the waves are represented, as done traditionally, in the form of a harmonic signal

$$v', w', u', p', \rho' (r, \varphi, x) = G\{(v, u, p, \rho)(r) \cos n\varphi; w(r) \sin n\varphi\} e^{\alpha x}. \quad (3.1)$$

Here v, w, u, p, and ρ are the amplitude functions of the waves; n is the wave number, characterizing the periodicity and number of vortices in the azimuthal direction, the mode of the wave; α is the longitudinal gain factor (α > 0 is the growth rate); G is the amplitude parameter, the weighting function. Equations (1.1) for the waves (3.1) assume the form

$$\begin{gathered} \alpha U v - 2Uu/R_0 + p_r/\rho_0 = 0, \quad \alpha U w - np/r\rho_0 = 0, \\ \alpha U u + (U_r + U/R_0) v + \alpha p/\rho_0 = 0, \quad \alpha U (p/a^2 - \rho) - \rho_{0r} v = 0, \\ \alpha U \rho + \rho_0 [v_r + nw/r + \alpha u + (1/r + 1/R_0 + \rho_{0r}/\rho_0) v] = 0. \end{gathered} \quad (3.2)$$

Outside the mixing layer v, w, u, p, ρ → 0.

The system reduces to a second-order ordinary differential equation for p:

$$\begin{gathered} p_{rr} + (1/r - 2F_r/F - \rho_{0r}/\rho_0) p_r + (\alpha^2 - n^2/r^2 - F^2/a^2) p = [(F(BB_1)_r - 2F_rBB_1)/FC - 2/R_0] p_r - \\ - [2(1/r + F_r/F - \rho_{0r}/\rho_0 - C_r/C + 1/R_0)/R_0 - BB_1 (F^2/a^2 + n^2/r^2)/F^2] p, \\ F = \alpha U, \quad B = 2U/R_0, \quad B_1 = U' + B/2, \quad C = F^2 + BB_1. \end{gathered} \quad (3.3)$$

The left-hand side represents the ordinary equation for disturbances without centrifugal forces; the right-hand side contains correction terms, proportional to $1/R_0$. In order to avoid singularities, arising in the solutions in regions where U → 0, nonstationary and spatial dependences are formally introduced into the equations, so that the solutions are actually constructed not for zero but rather quite low frequencies. Thus the acoustic Strouhal number, constructed according to the sound speed outside the jet, $Sh = 2\pi\omega\bar{r}_0/a$, was assumed to be 0.005 and 0.0025, corresponding to waves with period $T_t > 250$. The period of the spatial variations is $T_x > 100$. On the measurement section such waves can be regarded as stationary.

The boundary conditions for p, corresponding to solutions decaying outside the δ layer, were constructed using modified Bessel functions I_n and K_n of order n in regions where U = const [5]; it was assumed in so doing that the boundary conditions do not contain centrifugal effects:

$$\begin{gathered} r < r_2: p \sim I_n, \quad p_r \sim I_{nr} \quad (U = 1), \\ r > r_3: p \sim K_n, \quad p_r \sim K_{nr} \quad (U \sim 10^{-4}). \end{gathered} \quad (3.4)$$

Thus Eqs. (3.3) and (3.4) enable formulating the boundary-value problem for determining the eigenvalues α and n of T−G waves with prescribed values of R_0, M_0, and δ, and the system (3.2) enables finding the amplitude functions of these waves.

As noted in [5], numerical calculations have established that Eq. (3.3) gives several families of solutions satisfying the conditions (3.4). Additional modes (irregular, according to the terminology of [10]) appear. The behavior of five such branches of solutions was traced. Among them, there is a branch A on which the values of α depend on the characteristics of the flow (changes in δ and M_0) and the scale of the wave motion (values of n). The eigenvalues α for the families B, C, D, and E are completely conservative with respect to these parameters and are determined only by the curvature $1/R_0$. Figure 2 illustrates this thesis. Here the functions α(n) are presented for the branch A (solid lines) with R_0 = 25, 10, 8.5, and 5.5 (lines 1-4) with fixed flow parameters M_0 = 1.5 and δ = 0.15. It was found that excitations of higher-order modes (small-scale waves) should grow more intensely. This behavior is opposite to that of traveling disturbances, where it is large-scale oscillations that are more unstable. Increasing the curvature $1/R_0$, which results in stronger centrifugal effects, intensifies the instability of the wave process.

The solutions for the branches B, C, D, and E, written in order of increasing α, are given for R_0 = 5.5 (dashed lines) and 25 (dot-dash lines). It is evident that, on the whole, the growth rates for these branches exceed the values given by the family A, but there exist ranges of values of n where they are comparable. Under such conditions the problem of identifying waves according to whether or not they belong to a particular family becomes an important problem in the analysis of experimental data. In this connection there arises the problem of determining the value of R_0. This problem is exacerbated by the fact that the boundary of the layer is poorly recorded by experimental methods based on measurements performed with Pitot tubes in subsonic regions.

Completing this section on the dependences of the wave characteristics on the flow parameters, we point out that for the branch A the values of α decrease slightly as the thickness of the layer increases. As an example, we give the variant n = 20, R_0 = 5.5, and M_0 = 1.5. Here α = 1.8016 for δ = 0.15 and α = 1.73 for δ = 0.25. As the Mach number increases, the values of α decrease from 0.596 (M_0 = 1.5) to 0.563 (M_0 = 5) (n = 10, Sh = 0.0025, δ = 0.15). Variations of these parameters have a greater effect on the distributions of the amplitude functions of the waves (3.1).

4. Amplitude Functions of T–G Waves and the Structure of the Longitudinal Branches. They were studied in detail for solutions with branch A and the additional branch B. It was found that the form of the wave is determined mainly by the value of the azimuthal wave number n and the radius of curvature R_0 of the trajectories. The effect of the Mach number and the thickness of the layer is similar to that of the scale factors. Figure 3 displays distributions of the amplitude functions of the transverse v, azimuthal w, and longitudinal u velocity components for Sh = 0.005, R_0 = 5.5, n = 20, and δ_1 = 0.15 (lines 1) and δ_2 = 0.25 (lines 2) for the same intensity of the waves, as well as the values of the average velocities U near the outer boundary of the jet and the dimensions δ_1 and δ_2. It is interesting that the wave speeds are not high below the inner boundary of the mixing layer. At the same time, the upper boundary of the layer (low subsonic speeds) is disturbed quite strongly; here both longitudinal and rotational velocity components are observed. It is evident that the center of the longitudinal vortex for δ_1 is located at r ~ 1.1, while for δ_2 it can be hypothetically found in the near field, in the flooded space. The longitudinal velocity u is an order of magnitude higher than v and w. The wave intensity, calculated as $\varepsilon = (\langle u'^2 \rangle)^{1/2}$, is 17.5%; if, however, all three velocity components are considered, then this value decreases to 10%.

Solutions with the additional branches are also found to be very reasonable. This investigation made it possible to find some behavioral characteristics which are characteristic of this class of waves. They are summarized in Fig. 4, where the vortex configurations engendered by the vector field of velocities v' and w' for waves of different scales (different n) with R_0 = 25 are shown schematically. This characterization, from all appearances, contains all variants that can occur in jets. It was found that the vortex configurations exhibit several stages, which are the same for both families A and B, the solutions from B leading somewhat in this dynamics, waves from A.

For small n (large-scale oscillations) the stage of chaotic disoriented vorticity, when a wave still cannot form a vortex (Fig. 4a), is observed first. This stage is characteristic for n < 12 from A and for n < 6 from B. As n increases, a vortex forms in the flow and strongly disturbs the outer boundary of the layer and the external medium (Fig. 4b). The velocity distribution in such a configuration is displayed in Fig. 3 for δ_2 = 0.25. Further increase of n results in localization of such a solitary vortex in the layer δ. The vortex is centered in regions where U ~ 0.01 (Figs. 4c and 3 for δ_1 = 0.15). In all probability, it is for these values of U that R_0 should be determined. Such a stable vortex configuration is mainly realized for low values of R_0 for strong centrifugal forces. As n increases further (n ~ 22) this primary vortex is displaced into the exterior region δ, and there forms in the region of high velocities a second oppositely polarized vortex, so that two vortices (Karman vortices) coexist in the mixing region. The intensities of this pair equalize (Fig. 4d, e) quite rapidly (n ~ 30 for A). As n increases further, the stable configurations break down and small-scale modes (n $\gtrsim$ 50) lead to chaos in the flow, resulting in disoriented vorticity (Fig. 4f).

Figure 4 displays the amplitude functions of the longitudinal wave component u(r), which forms distortions of the average profile U(r). The form of the density profile ρ of the wave mainly repeats the form of u, but its maximum value is shifted into the region where the layer δ starts.

These are the preliminary basic data for harmonic T–G waves. Knowledge of these data made it possible to analyze the experimental information kindly provided by the authors of [1, 2].

5. Spectral Composition of the Observed Disturbances. As stated in [1, 2], the experimental measurements yielded azimuthal traces of the total pressure p_0 in different transverse and longitudinal positions of the first "barrel" of the jet. These traces are represented in the form of realizations, where quasiperiodic changes in pressure, forming sawtooth curves, called here variations δp_0 of the total pressure, were recorded against the background of average values of p_0. The quite complicated form of δp_0 is interesting; it is

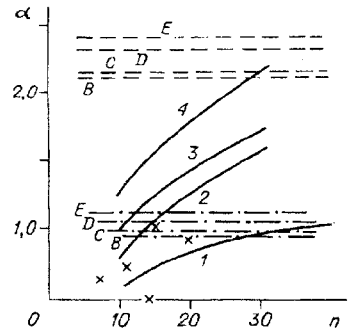

Fig. 2

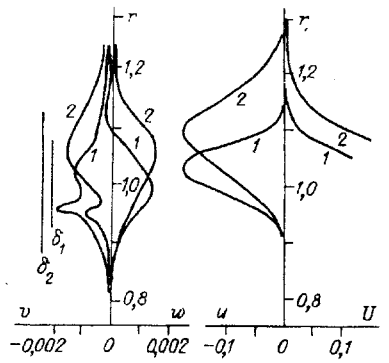

Fig. 3

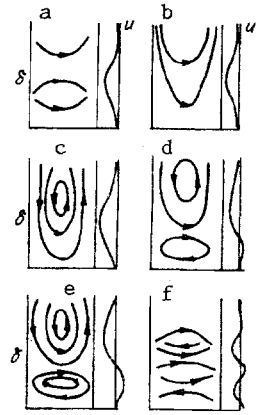

Fig. 4

characteristic of natural disturbances, which are always difficult to analyze. The first problem was to analyze and retrieve the signal δp_0 on the basis of analytical functions of the waves (3.1). For this, the formula

$$p_0/p_{st} = [1 + M^2(\varkappa - 1)/2]^{\varkappa/(\varkappa-1)}, \quad M^2 = U^2/a^2 = U^2\rho/\varkappa p$$

where all components can be calculated, for variations of the total pressure was derived up to quadratic terms from the gas-dynamic relation for the total pressure

$$\delta p_0/p_0 = \left[p'/p_{st} + \varkappa M^2\left(\frac{1-\varkappa}{\varkappa}\frac{p'}{p_{st}} + \frac{2u'}{U}\right) \Big/ (2 + (\varkappa - 1)M^2)\right]. \qquad (5.1)$$

In addition to an instrumental estimate of the spectral composition, made in [1, 2], the distributions δp_0 in different longitudinal positions were Fourier-analyzed numerically in order to find both the amplitude and phase relations of the constituents of this complicated signal so as to retrieve the signal numerically. This information is required in order to estimate the gains α and therefore to determine whether or not a wave belongs to one or another family.

In view of the fact that the amplitudes of the waves depend strongly on the transverse coordinate at quite small transverse distances, it was very important to maintain the referencing to the chosen reference points. These reference points can be the constancy of the average total pressure p_0 (tracing of a single streamline) or a point with a characteristic value of δp_0 (for example, the maximum value), and finally these must be the closest possible longitudinal sections, where R_0 remains constant, and the viscosity and nonlinearity cannot significantly affect the wave dynamics. In spite of the abundance of data obtained, only several realizations adequately meet these conditions.

The results of the analysis make it possible to interpret the dynamics and evolution of the wave process as follows. A wide spectrum of disturbances ($1 \leqslant n \leqslant 80$), having approximately the same intensity, is excited at the base of the jet. Figure 5 displays the amplitude and phase spectra δp_0 at x = 0.5, 1.5, and 2 ($x = \bar{x}/2\bar{r}_0$). The existence of quite strong waves with small values of n can be explained by the errors introduced by both the weak ellipticity of the nozzle and imperfections in the measurement procedures with circular passage around the nozzle as well as by oscillations of the total pressure in the mixing chamber during the measurements.

We now trace the dynamics of oscillations with $n > 9$. Some predominant modes, clustering near $n \sim 13$, 18, 25, 40, 55, and so on, can be identified among the disturbances, even for small values of x. We do not yet have an unequivocal answer concerning their genesis. They are equally likely to be a continuation of vortices associated with the inner gas-dynamics of the nozzle itself and with the fact that at such longitudinal distances selective intensification of oscillations associated with the roughness of the edges and nonuniformity of the flow at the cutoff has already occurred. The question also requires further analysis.

Farther downstream the evolution is associated with intensification of the modes $9 \leqslant n \leqslant 30$ and decay of high-frequency components. The latter components decay successively — modes with higher azimuthal numbers decay or are absorbed earlier. We consider in greater detail spectra with x = 1.5 and 2, which more than others satisfy conditions for determining the

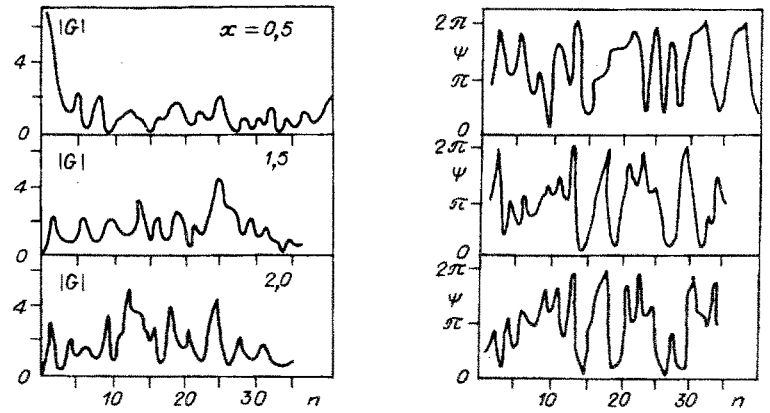

Fig. 5

constants α. The phase spectra show that for $10 \leqslant n \leqslant 30$ there is no strong nonlinear process accompanied by merging and capture; all modes retain their spatial orientation, though the exchange processes for them are different. It is possible to identify a group of decaying, constant, and growing modes.

Figure 2 displays (cross marks) the constants α, extracted from the spectrograms presented. Up to n ~ 20 the growth rates are described quite well by the computational relations for the branch A of the nonviscous approximation with $10 \leqslant R_0 < 25$. We point out that from the reference points of the suspended shock it was found that $R_0 \sim 6$, and according to the $p_{0\max}$ line $R_0 \sim 12$. For $n > 20$ processes which are not described by the nonviscous linear approximation start to influence the dynamics of the real components. Thus one of the predominant modes (n = 25) belongs to a group with $\alpha = 0$; for these longitudinal values of x it falls in the range of high-mode decaying components and the computed growth rates α for it can be compared only to the values obtained for spectrograms with $x < 1.5$. Such a comparison of the computed and experimental values of α shows that, first, their quite good agreement in the region of applicability of nonviscous linear approximation indicates that the model adequately describes the physical phenomenon and, second, the real dynamics of T–G waves can be described only by taking into account the viscous and nonlinear effects.

Let us assume that the other modes for which further calculations were performed also belong to this branch of the solutions, 14 spectral modes $4 \leqslant n \leqslant 28$ with amplitudes $|G| > 2$ for $M_0 = 1.5$, $\delta = 0.15$ with $R_0 = 5.5$, 8.5, and 10 were used as the basic modes. For them, the amplitude functions were determined according to Eq. (3.2) and the total signal

$$\delta p_0 = \sum_{i=1}^{14} G_i \delta p_{0i}(r) \cos(n_i\varphi - \psi_i)$$

was retrieved using Eq. (5.1).

All obtained variants were found to be quite close in value and similar in form, so that we present one of them for $\delta = 0.15$ and $R_0 = 8.5$. It is obvious that variation of these values should affect the transverse and not the azimuthal distributions of the wave characteristics. The retrieved signal δp_0 presented in Fig. 6 repeats quite accurately the characteristic features of the initial realization (point 4, Fig. 2 [1]), the periodicity in the alternations of maximum and minimum values is preserved, and the location of the maximummum values of δp_0 is described correctly. All this provides a basis for the assertion that the analytical form of the oscillations in the form of stationary T–G disturbances (3.1) is close to reality, and the agreement between the experimental and computational results can be improved by obtaining more accurate references with respect to the thicknesses of the layer, values of the radius of curvature R_0, and other assumptions adopted here. We look forward to progress in this field.

Figure 6 also displays the total functions of the wave velocities for a distinguished value of r over the entire circumference of the jet. The value r = 1.02 was chosen at the location where the longitudinal component of the velocity assumes its maximum vlaue. As is evident, the longitudinal velocity u' repeats the form of δp_0, since it is the value of u' that determines the form of δp_0. The dimensions of the oppositely polarized vortices, the components of vortex pairs, can be retrieved from the distributions of the velocities v' and w'. Their azimuthal extent is indicated in the figure, together with the conventional sign

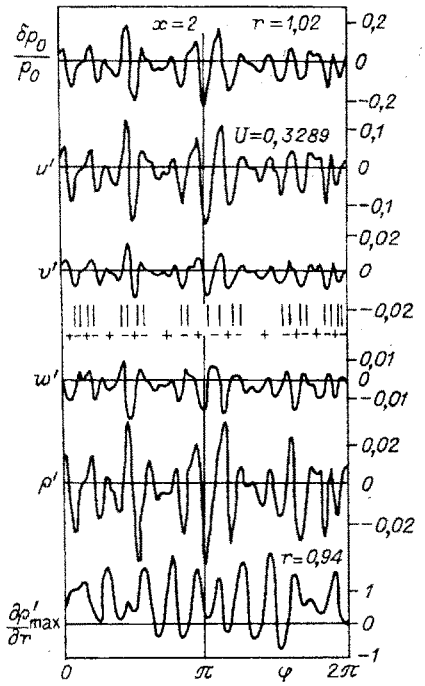

Fig. 6

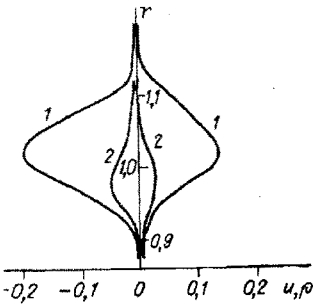

Fig. 7

of the vorticity. It is evident that the dimensions of the right- and left-rotating vortices in such pairs are different, and their vorticity is different; stagnant regions where there are no radial-azimuthal flows are also observed. The rotational components of the total T–G wave are an order of magnitude smaller than the longitudinal component. Of course, it should be expected that the characteristic radial component of the average profile V will introduce corrections into the computed picture of the vortex configurations.

Figure 6 displays the azimuthal distributions of the total perturbation density ρ', which correlate completely with the distributions u'. The decrease in u' is associated with low-head gas flowing into the layer from external regions; this produces a corresponding deformation of the average density and corresponds to negative values of ρ'. Finally, the figure also displays the values of the maximum gradients $\partial\rho'/\partial r$. It is well known that the maximum values of the optical gradients of the density, which can be directly associated to gradients of the real gas density, are recorded in the shadow photographs of jets (Toepler pictures). If the alternating peaks are identified with the dark bands in the photographs and the alternating troughs are associated to the light-colored bands, then the number of bands in the photographs and the number of peaks or troughs in the computed data can be counted accurately. This can give an additional possibility for calibrating the changes in optical density and retrieving the true values of ρ.

Figure 7 displays the transverse distributions of the longitudinal velocity and density at the phase of the minimum ($\varphi \sim 180°$) and the phase of the maximum ($\varphi \sim 202°$) for the total wave studied. It is evident that the maximum values of ρ fall in the range of higher flow velocities. Transverse distributions of this type are qualitatively similar to those presented in Fig. 3 of [1], though the absence of a line of average total pressure in the latter distributions makes it difficult to make an accurate comparison. The maximum intensity of the total T–G wave, calculated from the longitudinal velocity, is estimated to be 20%. The average profile U can be distorted by 20-40%.

This theoretical investigation, supplementing and explaining the experimental information, makes it possible to assert reliably that a coherent structure, produced by stationary Taylor–Görtler vortex waves, exists in the initial section of a supersonic nonisobaric jet.

We thank S. A. Gaponov and V. I. Merkulov for their interest in this work and for helpful discussions.

LITERATURE CITED

1. V. I. Zapryagaev, S. G. Mironov, and A. V. Solotchin, "Spectral composition of the wave numbers of longitudinal vortices and structural characteristics of flow in a supersonic jet," Prik. Mekh. Tekh. Fiz., No. 5 (1993).

2. V. I. Zapruagaev and A. V. Solotchin, "Measuring of wave number spectrum of coherent structures in supersonic underexpended jet," Proceedings of the International Conference on the Methods of Aerophysical Research, Part 2, Novosibirsk (1992).
3. N. A. Zheltukhin, V. I. Zapryagaev, A. V. Solotchin, and N. M. Terekhova, "Spectral composition and structure of stationary Taylor–Görtler vortex perturbations of supersonic underexpanded jet," Dokl. Ross. Akad. Nauk, 325, No. 6 (1992).
4. N. A. Zheltukhin and N. M. Terekhova, "Modelling of stationary longitudinal vorticity in initial section of supersonic jet," in: Proceedings of the International Conference on the Methods of Aerophysical Research, Part 2, Novosibirsk (1992).
5. N. A. Zheltukhin and N. M. Terekhova, "Perturbations of high modes in a supersonic jet," Prik. Mekh. Tekh. Fiz., No. 2 (1990).
6. J. M. Florian, "On the Görtler instability of boundary layers," Prog. Aerospace Sci., 28, 235 (1991).
7. G. N. Abramovich, T. A. Girshovich, S. Yu. Krasheninnikov, et al., Theory of Turbulent Jets [in Russian], 2nd edn., Nauka, Moscow (1984).
8. P. J. Morris and C. K. W. Tam, "Near and far fields noise from large scale instability of axisymmetric jets," AIAA Paper No. 77-1351, New York (1977).
9. V. S. Avduevskii, A. V. Ivanov, I. M. Karpman, et al., "Structure of turbulent underexpanded jets effluxing into a flooded space and the comoving flow," Izv. Akad. Nauk SSSR, Mekh. Zhid. Gaza, No. 3 (1972).
10. A. Michalke, "Survey on jet instability theory," Prog. Aerospace Sci., 21, 159 (1984).

STATIONARY CURRENTS IN OSCILLATING FLOWS IN TUBES IN THE CASE OF QUASISTATIONARY TURBULENCE

E. I. Permyakov

UDC 532.517.4:534.213

It is well known that stationary flows are generated during the excitation of standing waves in resonators [1], substantially affecting heat and mass transfer [2, 3]. In the literature one can find a set of specific results in this field of study, but their range of application is comparatively narrow.

We clarify what we have in mind. Consider flows in resonating tubes. In the case of oscillating flows the current is characterized by two criteria: one usually uses the Strouhal number $Sh = 2R\omega/u_m$ and oscillation Reynolds number $Re_c = 2Ru_m/\nu$ (R is the tube radius, ω is the cyclic oscillation frequency, u_m is the velocity oscillation amplitude, and ν is the kinematic viscosity). In the Re_c–Sh plane one can indicate three regions: I – the laminar flow regions (in which are located all results available in the literature), II – the region of turbulent flows, in which the nonstationary character of turbulence is substantial, and III – the region in which turbulence can be assumed to be quasistationary (Fig. 1). The boundaries of these regions are curves 1 and 2, respectively, for

$$Sh = Re_c/160\,000; \quad (1)$$

$$Sh = 0{,}158/Re_c^{0.25} \quad (2)$$

The boundary (1) was obtained as a result of generalizing the experimental and theoretical data of [4], and that of (2) is the result of theoretical analysis [5]. The boundary (2) corresponds to the condition $Z = 4R\omega/\lambda u_m < 1$, where λ is the hydraulic resistance coefficient, and the dependence $\lambda(Re_c)$ in (2) is taken from the Blasius law for smooth-walled tubes [6]. Obviously, the broadening of the investigated region of secondary flows requires taking into account the possible flow turbulization.

In the present study we investigate theoretically stationary flows in the case of quasistationary turbulence, i.e., in region III, which can be extended substantially if the tube walls are rough, i.e., if $\lambda = \text{const}$ [6].

Kazan'. Translated from Prikladnaya Mekhanika i Tekhnicheskaya Fizika, No. 5, pp. 56-62, September-October, 1993. Original article submitted February 19, 1992; revision submitted August 19, 1992.

